Article

Experimental Study of Piezoelectric Control for Changing Tilting Pad Journal Bearing Circumferential Angle and Radial Displacement

Shuxia Peng [1], Xin Qin [2], Xiaojing Wang [1,*], Guangyao Huang [1] and Xin Xiong [1]

1 School of Mechatronic Engineering and Automation, Shanghai University, Shanghai 200444, China; shxpeng@shu.edu.cn (S.P.); h1604948122@163.com (G.H.); xxiong@shu.edu.cn (X.X.)
2 Shanghai Marine Equipment Research Institute, Shanghai 200031, China; qinxin1313@163.com
* Correspondence: xjwangshu@126.com

Abstract: In order to improve the vibration performance of the oil-lubricated tilting pad bearing system, an experimental approach using a piezoelectric actuator to control two new flexible tilting pads is proposed. The performance test bench of the bearing–rotor system based on a tilting pad bearing with a flexible support is established. The different circumferential angles of the angle bearing tilting pad and the radial displacement of the displacement bearing are tested by a piezoelectric actuator. At the same time, the trajectory of the rotor center under actual operating conditions is analyzed. The experimental results show that the amplitude of the rotor journal can be significantly reduced by controlling the control variables related to the circumferential angle and radial displacement of the bearing bush. Therefore, this control improvement can improve the vibration performance of two new flexible tilting pad bearing–rotor systems. The technical means are provided for the active control of an oil-lubricated tilting pad bearing.

Keywords: axis center orbit; tilting pad bearings; piezoelectric actuator; rotor system; vibration

1. Introduction

Due to the highly stable adaptive adjustment performance of tilting pad bearings [1,2], which can improve stability, they have been widely applied in high-speed rotating machinery. However, the comparative complexity of their structure and assembly leads to heightened manufacturing costs. Furthermore, system vibrations, bearing wear, and the potential for severe safety incidents are exacerbated by faults such as rotor imbalance and misalignment [3].

System stability has been enhanced by numerous scholars through the alteration of the structure of tilting pad bearings. For instance, the conversion of unstable load-bearing pads into a fixed pad structure has been shown to decrease rotor vibration during operation when compared to conventional tilting pad bearings operating under identical parameters [4]. Alternatively, by modifying the pivot of the bearing pads with a flexible hinge support, the bearing structure can be simplified while still maintaining the exceptional performance characteristics of standard tilting pad bearings [5–7]. The essence of these innovations lies in the application of conventional passive control techniques to mitigate vibrations in rotor systems. Despite this, the spindle remains susceptible to vibrations caused by external stimuli or inherent residual imbalances when exposed to high-speed or ultra-high-speed rotations. Consequently, it is imperative to implement external control measures in order to effectively mitigate vibrations.

Currently, control methods mainly include electromagnetic control, hydraulic control, and piezoelectric control, among others [8,9]. For example, Das et al. [10] used electromagnetic actuators in flexible rotor bearing systems to apply control forces in two perpendicular directions on the rotor section, implementing the active control of spindle

vibration. The results of the numerical fitting showed an improvement in the system's unstable speed. Silva et al. [11] installed the electromagnetic actuator in the bearing box behind the bearing pad and applied electromagnetic force on the bearing pad, causing them to change their angular position relative to the bearing to improve the stability of the system. Oil- or water-lubricated bearings are usually connected to servo valves and hydraulic servo systems [12–14], while gas- or air-lubricated bearings use piezoelectric actuators and pneumatic systems [15–17] to adjust the angle or gap of the bearing bush.

Santos et al. [18–20] developed and tested two different forms of tilting pad journal bearings, adjusting the pressure and flow of actively injected lubricating oil along the radial direction of the bearing pad using piezoelectric devices, thereby changing the oil film pressure of the bearing. By changing the voltage of the piezoelectric device based on the measured vibration level, the vibration amplitude of the rotor during operation is reduced. Similarly, by injecting pressure oil into the bearing clearance through holes machined on the bearing sliding surface, the radial displacement between the bearing pad and the rotor is adjusted, and the pressure and flow of the lubricating oil supplied to the tilting pad bearing are controlled by a proportional-integral-derivative (PID) controller. The calculation analysis found that using a PID active lubrication control system can effectively control the vibration amplitude of the rotor, thereby adjusting the vibration amplitude and noise of the rotor [21,22]. Chasalevris et al. [23] used the vibration suppression of discontinuous spring characteristics and the passive radial displacement of the movable bearing half ring due to the additional liquid film, and the effective damping and stiffness coefficient of the bearing changed, thereby reducing the resonance amplitude. Deckler et al. [24] established a linear model to simulate the radial movement of a tile caused by a piezoelectric actuator in order to verify the effectiveness of the feedback control. The results showed that certain design parameters in the quadratic performance index can be used to determine the stiffness and damping of the closed-loop bearing system, thus allowing for the appropriate adjustment of the axis track. Da Silveira et al. [25,26] analyzed the feasibility of piezoelectric collector coupling on tilt pad bearings, verified that piezoelectric collectors can be assembled on the bearing without compromising the dynamic behavior, and determined that the harvested energy is sufficient for condition monitoring sensors. Yan et al. [27] established an optimal control model by embedding the piezoelectric actuator into two pivots of each tilting pad bearing. When the voltage is applied to the actuator, the tile can generate small displacements behind its radial pivot to change the air film force between the surface journal and the tile. Numerical control results showed that this optimal control system can effectively suppress the unbalanced response of the system. The control of the bearing pad angles has found effective applications in various bearing structures. Mizumoto et al. [28] embedded a piezoelectric actuator in each elastic region on the surface of a tilting pad gas bearing to deform the bearing surface and form a wedge-shaped region in the air gap. The experimental results show that with the increase of the applied voltage to the piezoelectric actuator, the wedge angle on the bearing surface increases, and the generated aerodynamic force causes the main shaft to displace, thereby suppressing the vibration of the main shaft. Chang et al. [29] conducted experimental tests on the nonlinear axial trajectory of a flexible hinge tilting pad bearing and controlled the swing angle of the bearing pad using a piezoelectric actuator device, obtaining the actual nonlinear axial trajectory under operating conditions. Wang et al. [30] provided two methods and examples to suppress the axial vibration in tilting pad bearings by installing embedded piezoelectric ceramic actuators on the back of the bearing pad to control the swing angle of the bearing pad. The numerical calculation results show that both control methods can achieve the goal of reducing the axial vibration. Chen et al. [31] employed a technique where piezoelectric ceramic actuators were positioned within grooves on the surface of the oil seal of a tilting pad bearing to adjust the clearance or preload coefficient of the bearing pads. The experimental outcomes from this study indicated that utilizing piezoelectric transducers (PZT) as actuators can effectively enable the active control of the bearing vibration. Qin et al. [32] proposed a method to actively control the radial displacement and circumferential

angle of the tilting pad of a hydrodynamic journal bearing. The theoretical research results show that increasing the control of the radial displacement and circumferential angle of the pad can effectively reduce the rotor journal amplitude and improve the operational stability of the bearing–rotor system. Girish et al. [33] also simulated the controlled motion of each tilting pad when they are controlled at equal positions, where the pads translate along the radial direction and tilt. The results show that the negative adjustment of the radial and pad tilt motion can generate an improved stability margin at higher eccentricity.

The angle control of the bearing has been proven to reduce the rotor vibration in experimental studies of tilting pad gas bearings and flexible hinge tilting pad bearings. This paper proposes the direct piezoelectric control of the radial displacement and circumferential angle of the oil film bearing, which has the advantages of a fast response, high precision, and high stability. Through pushing the radial displacement of the bearing, the clearance caused by wear can be reduced, thereby changing the oil film pressure. Pushing the circumferential angle of the bearing can increase the lubricating wedge gap and improve the smooth operation of the bearing.

Oil- or water-lubricated bearings are usually connected to servo valves and hydraulic servo systems to change the angular position of the bearing bush. The radial displacement between the bearing bush and the rotor is adjusted by injecting pressure oil into the bearing clearance through a hole machined on the bearing sliding surface. Gas- or air-lubricated bearings use piezoelectric actuators and pneumatic systems to adjust the swing angle of the bearing and the bearing clearance. In this paper, a piezoelectric actuator is used to control the oil-lubricated bearing, and the different circumferential angles and radial displacements of the two kinds of elastic-supported tilting tile bearings are adjusted. This changes the internal geometric parameters of the bearing, provides a technical means for the active control of the oil-lubricated tilting tile bearing, and improves the vibration performance of the bearing–rotor system.

2. Experimental Procedure

2.1. Test Bearings

The designed flexible supports for the tilting pad bearings in this study come in two forms: One is the angle-controlled bearing, referred to as the angle bearing. It was equipped with a pair of asymmetrically arranged springs with a stiffness of approximately 2.97×10^6 N/m. These springs not only induce circumferential deflection, but also provide certain radial stiffness. Two piezoelectric actuators were installed at the ends of the two main bearing pads, which were, respectively, arranged in the left and right 17° directions of the lower bearing pads, as illustrated in Figure 1a. This deliberate placement ensures that the piezoelectric actuators have the optimal range of motion to drive the angle of the bearing pads to its maximum extent. The other type involves a displacement-controlled bearing, referred to as the displacement bearing. This configuration comprises a dual-layer spring support system. The inner layer features an identical arrangement of asymmetric springs, while the outer layer consists of symmetrically positioned springs. The combined stiffness of this double-layered spring system is approximately 1.61×10^6 N/m. Two piezoelectric actuators were applied to the fulcrum position in the middle of the inner layer spring of the bearing pads, which were, respectively, arranged in the left and right 45° directions of the lower bearing pads, as shown in Figure 1b, so that the piezoelectric actuator could directly adjust the radial displacement of the bearing pads.

The two forms of tilting pad bearings were crafted through wire-cut electric discharge machining, achieving a unified structural design. This integration greatly reduced installation errors and enhanced installation precision. It is worth noting that the installation method of the piezoelectric actuators in the aforementioned two bearing types might compromise a portion of the spring elasticity. The fundamental parameters of the bearings are presented in Table 1.
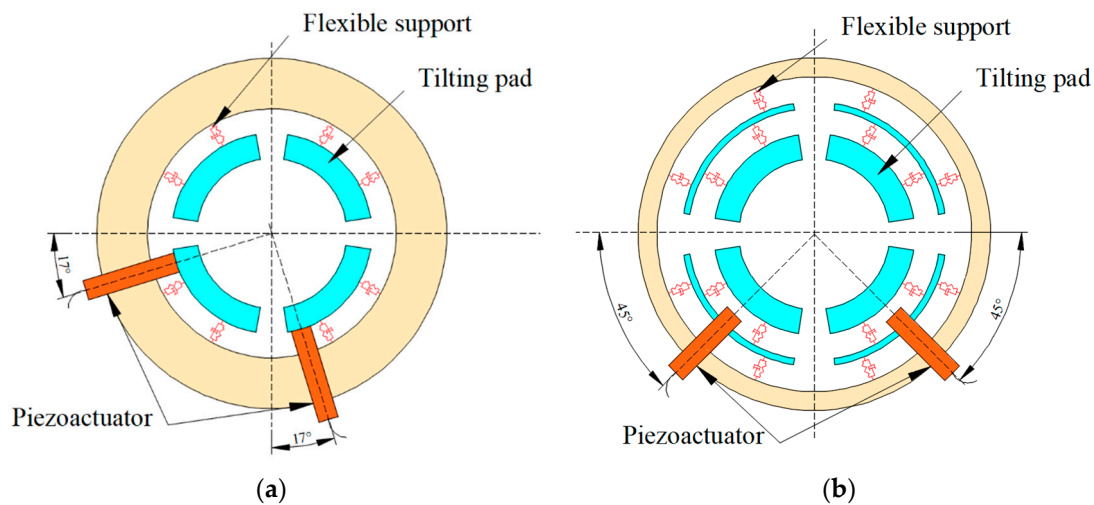
Figure 1. Implementation method of control: (**a**) angle bearing, (**b**) displacement bearing.

Table 1. Design parameters of the bearing specimens.

Parameters	Angle Bearing/Displacement Bearing
Bearing pad radius (R), mm	15.05
Bearing length (B), mm	25
Manufactured diameter clearance (c), mm	0.1
Preload factor (m)	0.375
Pad arc angle (°)	70
Number of pads	4
Thickness of pads (t), mm	5

2.2. Experimental Setup

The rotor–bearing system depicted in Figure 2 serves as the experimental test apparatus [34]. The rotor system consists of a flexible main shaft supported by a pair of test bearings and driven by a variable-speed electric main spindle via a flexible coupling. The high-speed electric motor is affixed to an adjustable position frame and is cooled by a circulating water cooling system, offering a rotational speed range of 0–12,000 rpm. The oil supply system comprises a 5 L oil tank, an oil pump, and an oil supply return pipeline, delivering a stable oil pressure of 0.1 MPa. This oil supply system ensures a consistent lubricating oil flow to the test system. As the shaft initiates rotation, a hydrodynamic film forms between the test bearings and the rotating shaft, generating an oil film force to support the rotor system. The water circulation system, oil station, and electric main spindle speed are controlled and displayed via a control console. The selected eddy current displacement sensor (Zhuzhou Liulingba Technology & Science Co., Ltd., Zhuzhou, China) is of the TR81 model: 810503, with a sensitivity of (±5%) 5 V/mm. Two eddy current sensors are mutually perpendicularly fixed to measure the displacement at the center of the disk. The selected acceleration sensor(PCB Piezotronics, Depew, NY, USA) is a piezoelectric accelerometer with an integrated signal conditioning circuit (ICP type). Its model is PCB Model: 352C33. These sensors were installed at the remote motor and bearing the pedestal, positioned both vertically and horizontally. The Bruel & Kjaer PULSE signal acquisition and processing system(B&K, Virum, Denmark) are employed to simultaneously monitor the rotor acceleration and displacement curves. The sampling frequency for collecting acceleration signals is 32,762 Hz, and a total of 16,384 signals are collected within 0.5 s. The sampling frequency for collecting displacement signals is 2560 Hz, and a total of 2048 data are collected within 0.8 s. Specific parameters of the dual-disk rotor system are presented in Table 2.
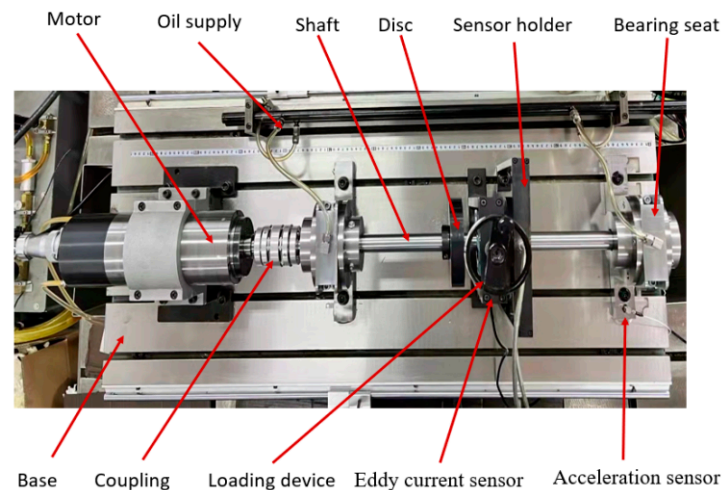
Figure 2. Bearing–rotor test bench.

Table 2. Parameters of the two-disk rotor.

Parameters	Value
Young's modulus (E), GPa	210
Density (ρ), kg/m^3	7850
Poisson's ratio (μ)	0.3
Shaft diameter (d), mm	30
Shaft length (L), mm	750
Mass of disk (m), kg	5.76
Mass of shaft (M), kg	4.17
Supply oil pressure (P), MPa	0.1
Type of lubricant	ISO-VG32
Oil inlet temperature (°C)	35

The piezoelectric actuator (Harbin Core Tomorrow Science & Technology Co., Ltd., Heilongjiang, China) model used in this test is PSt150/5/140VS10, equipped with XE-501c controller(Harbin Core Tomorrow Science & Technology Co., Ltd., Heilongjiang, China). The factory parameters are as follows: initial length $l0$ = 46 mm, maximum driving voltage 10 V, rated starting force 500 N, and rated stroke 40 ($\pm$10%) μm. In this paper, the operating range of the piezoelectric actuator is very small. The relationship between voltage and elongation is reduced to a linear relationship. Static calibration experiments were performed on both bearings to confirm the relationship between input voltage and pad deformation. The installation position of the piezoelectric actuator is shown in Figure 1, and the dial indicator is used to detect the swing angle of the tile in real time. The test is performed by applying a specific voltage range (from 0 V to 5 V in 0.5 V steps) to the piezo actuator. The dial gauge value was recorded 3 times and the average value was taken. The result is shown in Figure 3a. It can be seen that the change of the swing angle of the angular bearing is almost linear with the voltage applied to the piezoelectric actuator. Similarly, the relationship between the radial displacement change of the bearing pad of the displacement bearing and the voltage applied to the piezoelectric actuator is obtained, as shown in Figure 3b. It should be noted that the force on the bearing pad in this study is the resultant force of the piezoelectric actuator thrust and the spring force.
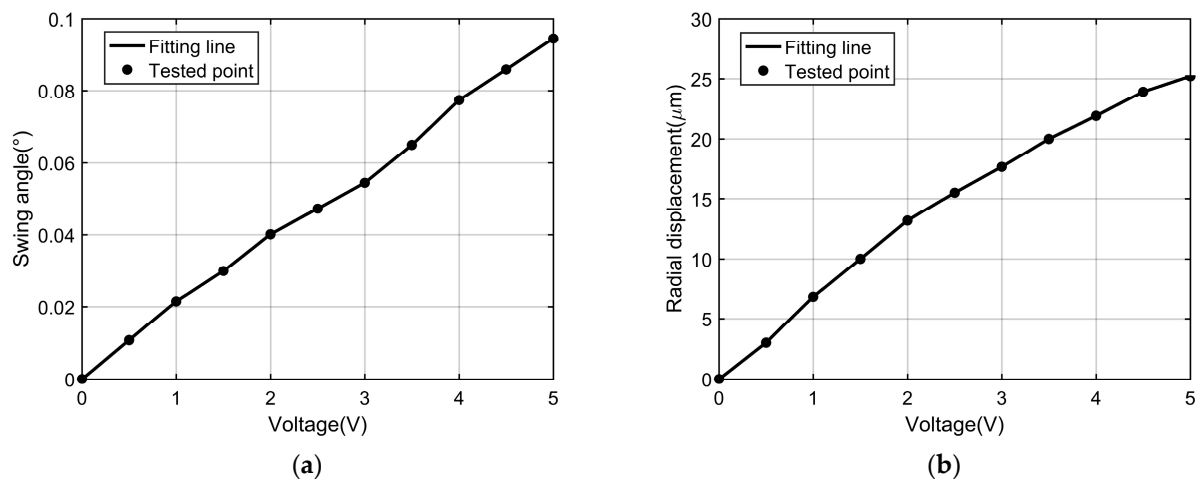
Figure 3. Relationship between deformation of the pads and voltage applied to the piezo-actuators: (**a**) angle bearing, (**b**) displacement bearing.

3. Control of Tilting Pad Bearing–Rotor System

A comparative analysis was carried out between the angle bearings and displacement bearings with the application and absence of piezoelectric actuators. Voltage signals of 0.5 V, 1 V, and 2 V were applied to the piezoelectric actuators, resulting in controlled angle and displacement outputs, as outlined in Table 3.

Table 3. Deformation of bearing shells under different piezoelectric voltage controls.

Piezoelectric Voltage (V)	Control Angle (°)	Control Displacement (μm)
0.5	0.011	3.01
1	0.021	6.83
2	0.040	13.17

3.1. Experimental Results of Angle Bearing Control

By adjusting the rotation speed of the electric spindle, a set of steady-state signals was collected every 500 rpm from 1000 rpm until 6000 rpm. Fast Fourier transform is performed on the acceleration time-domain signal collected when the angular bearing is supported, and a waterfall diagram is drawn. It can clearly describe the trend of the acceleration vibration amplitude changing with the speed, and it can also be used to describe the synchronous vibration of the rotor and the asynchronous vibration caused by the oil film [35,36]. Figure 4 shows the vibration acceleration waterfall diagram of the angle bearing machine foot in the horizontal direction. It can be seen from the waterfall diagram that as the speed increases, the amplitude of the fundamental frequency (1×) of the rotor vibration gradually increases, and after reaching the peak value, it shows a downward trend followed by an upward trend. The peak amplitude of the angular bearings appears around 4500 rpm.

On this basis, the angle bearing was controlled, and the experimental results of the four control voltages were compared, which were 0 V when not controlled, and 0.5 V, 1 V, and 2 V controlled, corresponding to the angle control 0°, 0.011°, 0.021°, and 0.040°. Figure 5 is a comparison diagram of the axis trajectory of the rotor system at different speeds under different control voltages. It can be seen that at 4000 rpm, the stability of the rotor system under control is significantly higher than that under no control, but there is little difference in the axis trajectory under different control angles. At 5000 rpm and 6000 rpm, the area of the axis track under control is also significantly smaller than that of the uncontrolled one, and with the increase in the control angle, the area of the axis track is further reduced, and the axis track gradually tends to be circular. System stability is further improved. The experimental results of the axis trajectory show that the vibration level of the system can be reduced by controlling the angle of the propulsion bearing pad

and changing the stiffness and damping characteristics of the bearing. This is because as the angle control of the bearing pad increases, the wedge shape between the bearing pad and the rotating shaft becomes steeper, which will improve the pressure distribution and bearing capacity, and the stiffness and damping characteristics will also be improved to a certain extent, making the shaft center trajectory closer to the bearing center.
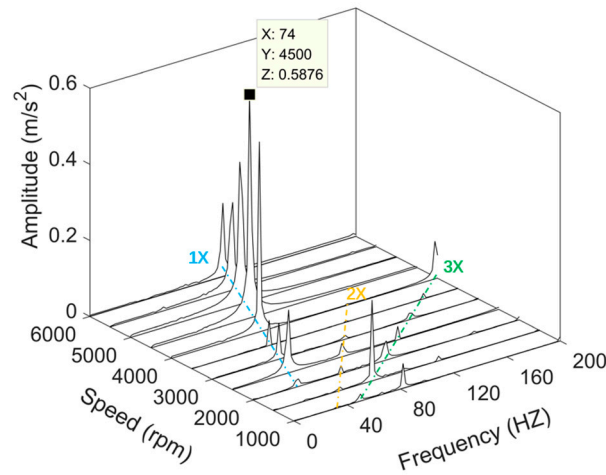

Figure 4. Waterfall plot of angle bearing vibration acceleration amplitude.

(a)

(b)

(c)
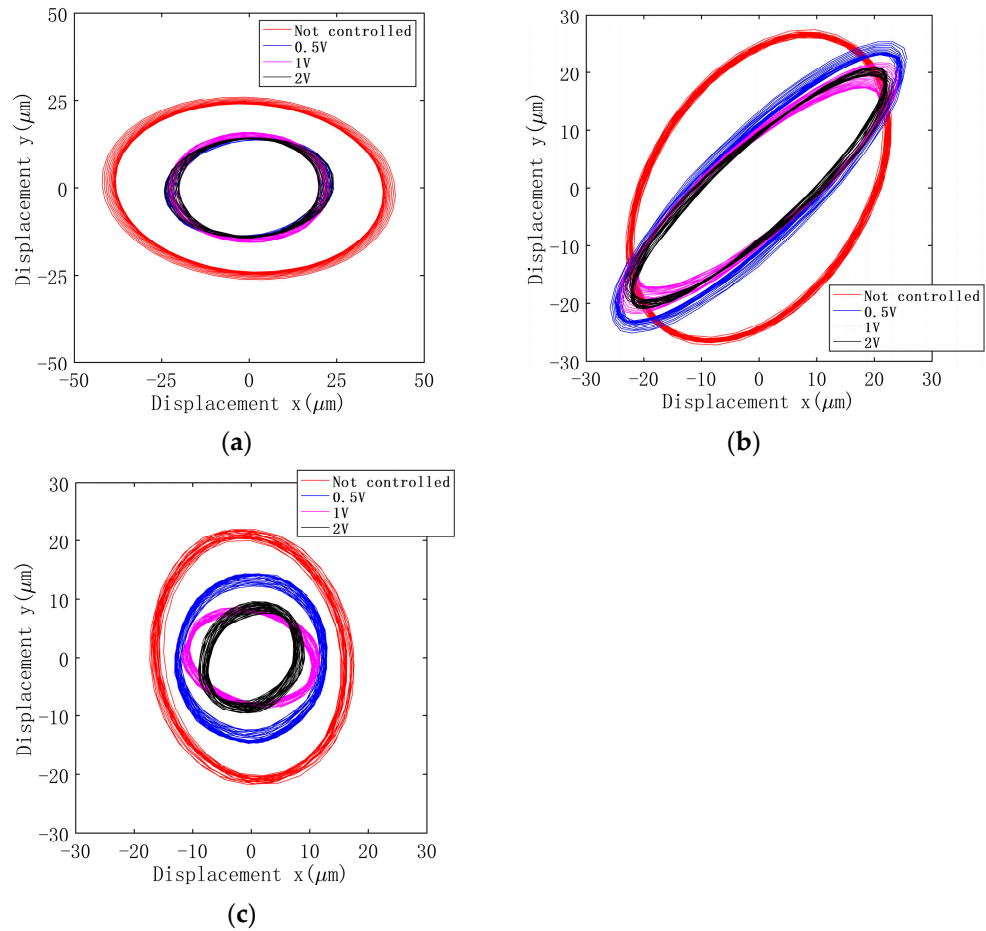
Figure 5. Comparison of axis trajectories with different control angles. (**a**) 4000 rpm; (**b**) 5000 rpm; (**c**) 6000 rpm.

In order to further study the stability of different journal bearings at specific speeds, the corresponding spectograms at different speeds were also drawn, as shown in Figures 6–8. It is worth noting that the amplitude in the spectrum refers to the axial displacement in the y direction. The maximum amplitude of the disk response under different control angles is plotted in Figure 9. At 6000 rpm, the peak value of the displacement at the fundamental frequency decreases with the increase in the control angle, the stability gradually improves, the degree of the reduction of the displacement amplitude is more obvious, and the maximum amplitude of the angle bearing is reduced by 62%. At 4000 rpm, the peak value of displacement at the fundamental frequency also decreases with the increase in the control angle, but the range of change is small, and the maximum amplitude decreases by 42% at 4000 rpm. At 5000 rpm, the magnitude of the fundamental frequency of the displacement decreases with the increase in the control angle, but the magnitude of the decrease is not as good as other rotational speeds. In general, the increase in the control angle of the load-carrying shoe makes the amplitude of the fundamental frequency lower, thereby improving the stability of the rotor system.
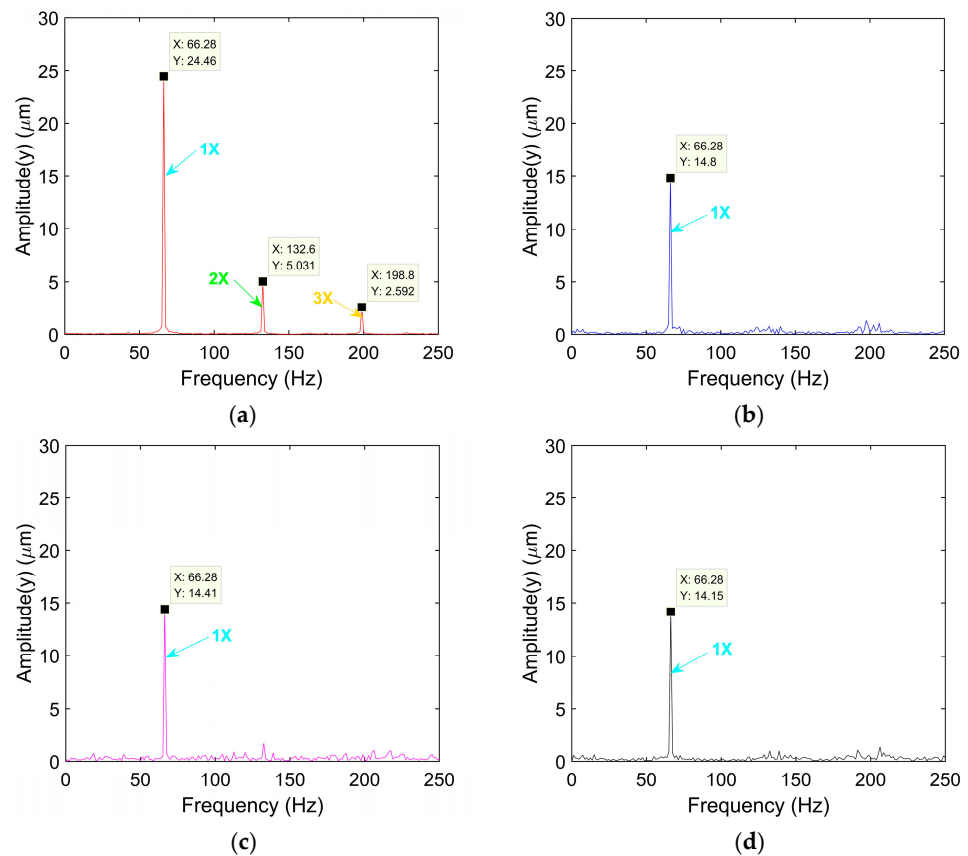

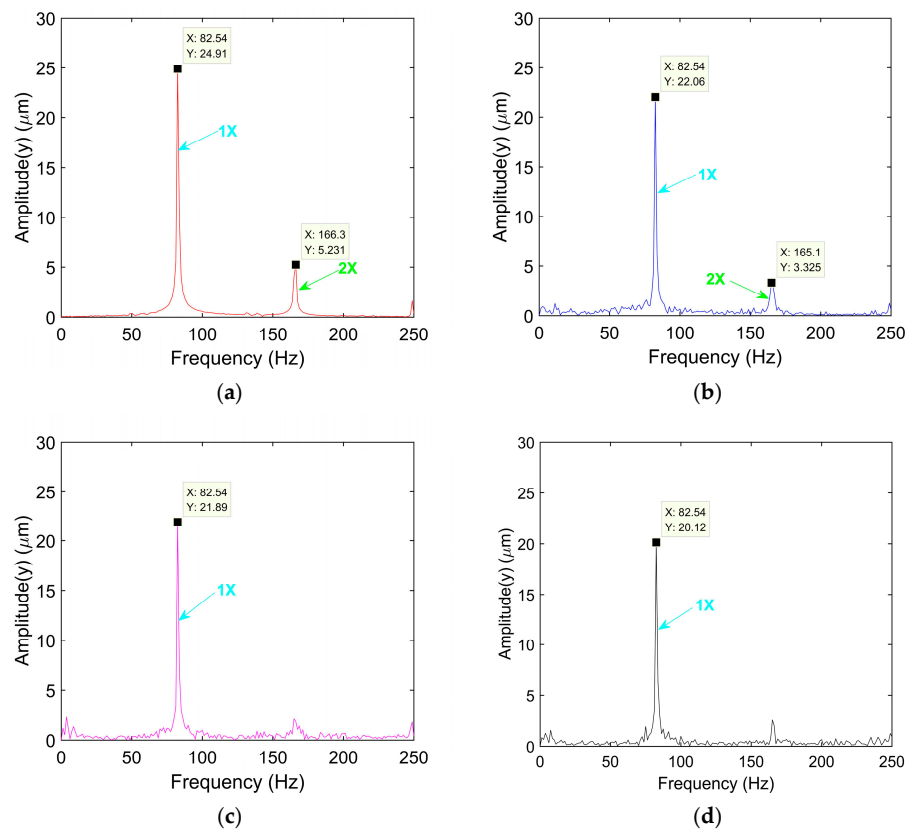**Figure 6.** Displacement spectrum at 4000 rpm under different control angles. (**a**) Not controlled; (**b**) 0.5 V; (**c**) 1 V; (**d**) 2 V.

Figure 7. Displacement spectrum at 5000 rpm under different control angles. (**a**) Not controlled; (**b**) 0.5 V; (**c**) 1 V; (**d**) 2 V.
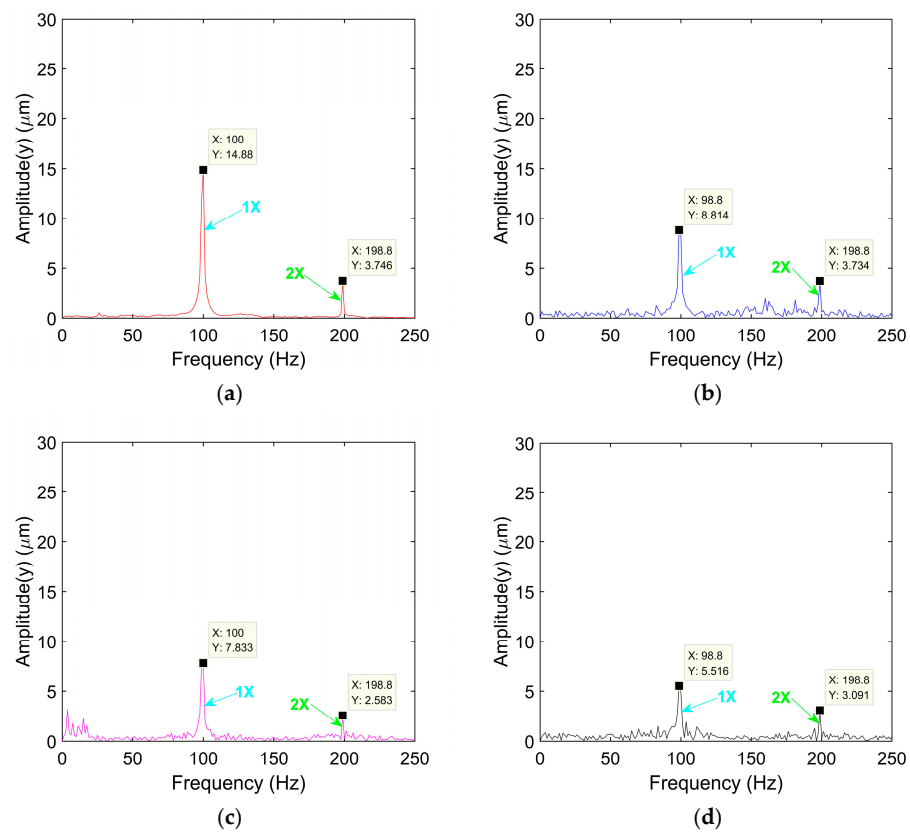

Figure 8. Displacement spectrum at 6000 rpm under different control angles. (**a**) Not controlled; (**b**) 0.5 V; (**c**) 1 V; (**d**) 2 V.
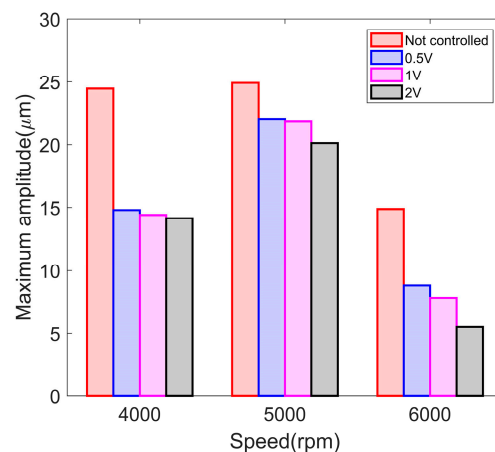
Figure 9. The maximum amplitude of the disk response under different control angles.

3.2. Experimental Results of Displacement Bearing Control

The acceleration time-domain signals for the displacement-supported bearing were also obtained, and their fast Fourier transforms were performed, resulting in the waterfall plot shown in Figure 10. Similar to the angle bearing, as the rotational speed increases, the amplitude of the vibration's fundamental frequency ($1\times$) gradually increases, reaching a peak and then decreasing before rising again. The peak amplitude of the displacement-supported bearing occurs at 4000 rpm, which differs from the peak amplitude location of the angular-supported bearing. This difference is attributed to the variation in bearing stiffness, as the dual-layer spring structure of the displacement-supported bearing reduces the overall bearing stiffness, leading to an earlier occurrence of the critical speed.
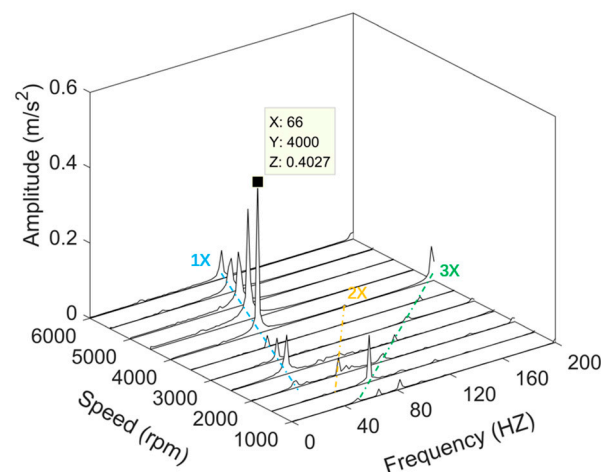

Figure 10. Waterfall plot of displacement bearing vibration acceleration amplitude.

Voltage signals of 0.5 V, 1 V, and 2 V are applied to the piezoelectric actuator, and output displacements of 3.01 μm, 6.83 μm, and 13.17 μm, respectively. Similarly, the orbit diagram of the rotational speed (4000–6000 rpm) near the peak amplitude of the displacement bearing and the frequency spectrum diagram of different control displacements at the corresponding rotational speed are drawn, as shown in Figures 11–14. As shown in Figure 11, in the same configuration, the track differences observed in Figures 5a–c and 11a–c at 4000, 5000, and 6000 rpm are due to differences in the bearing construction. Specifically, the stiffness of the two bearings is different, resulting in the track difference observed between the two in the zero-voltage state. When the rotor speeds are 4000 rpm and 5000 rpm, the area of the shaft center orbit gradually decreases with the increase in the displacement control of the 30 bearing pad, and the differences in the shaft center orbit become more pronounced under different control voltages. At 6000 rpm, the shaft center

orbit under control is more distinct compared to the uncontrolled condition, indicating further improvement in rotor system stability. However, there is little difference in the shaft center orbit under different control voltages, with the smallest area observed at a control voltage of 2 V. This is because the displacement of the bearing pad reduces the bearing radius clearance, thereby decreasing the oil film thickness and increasing the oil film pressure and load-carrying capacity. This leads to an improvement in bearing stiffness and damping characteristics, resulting in the shaft center orbit moving closer to the bearing center, thus enhancing the operational stability of the system.

As depicted in Figures 12–14, at various rotational speeds, the fundamental frequency amplitude of the rotor system diminishes with the augmentation of the controlled radial displacement of the bearing pads. The maximum amplitude of the disk response under different control displacements is plotted in Figure 15. Among these, the effect of reducing the amplitude is most pronounced at 6000 rpm, with the maximum amplitude decreasing by 54% when the displacement is controlled at 2 V. At 4000 rpm and 5000 rpm, the maximum amplitudes are reduced by 33% and 25%, respectively, consistent with the experimental results of the shaft center orbit. It is worth noting that at 6000 rpm, the displacement bearing controlled by a piezoelectric actuator with a driving voltage of 2 V exhibits the lowest fundamental frequency, but the second harmonic is the highest.
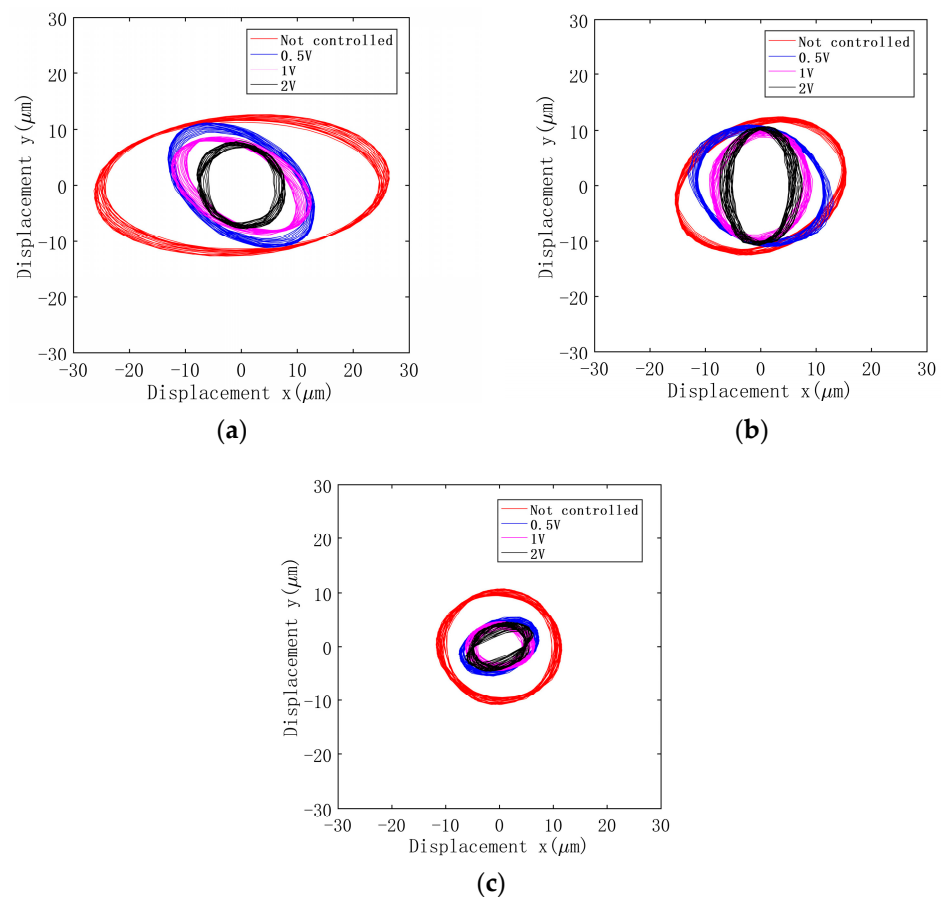

Figure 11. Comparison of axis trajectories with different control displacements. (**a**) 4000 rpm; (**b**) 5000 rpm; (**c**) 6000 rpm.
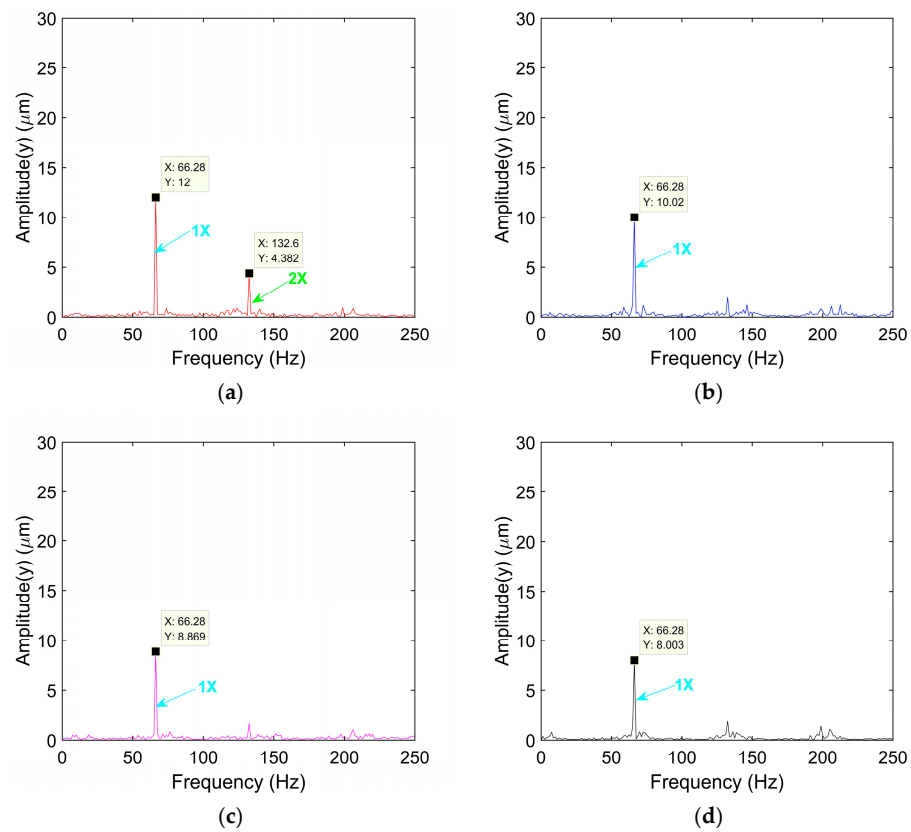
Figure 12. Displacement spectrum at 4000 rpm under different control displacements. (**a**) Not controlled; (**b**) 0.5 V; (**c**) 1 V; (**d**) 2 V.
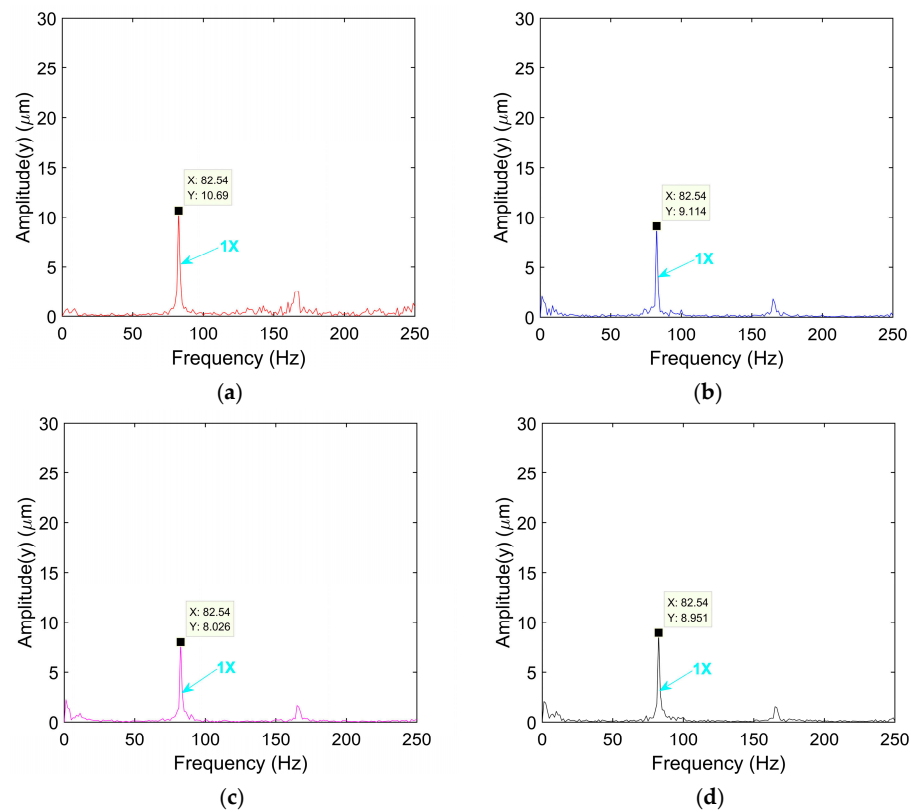

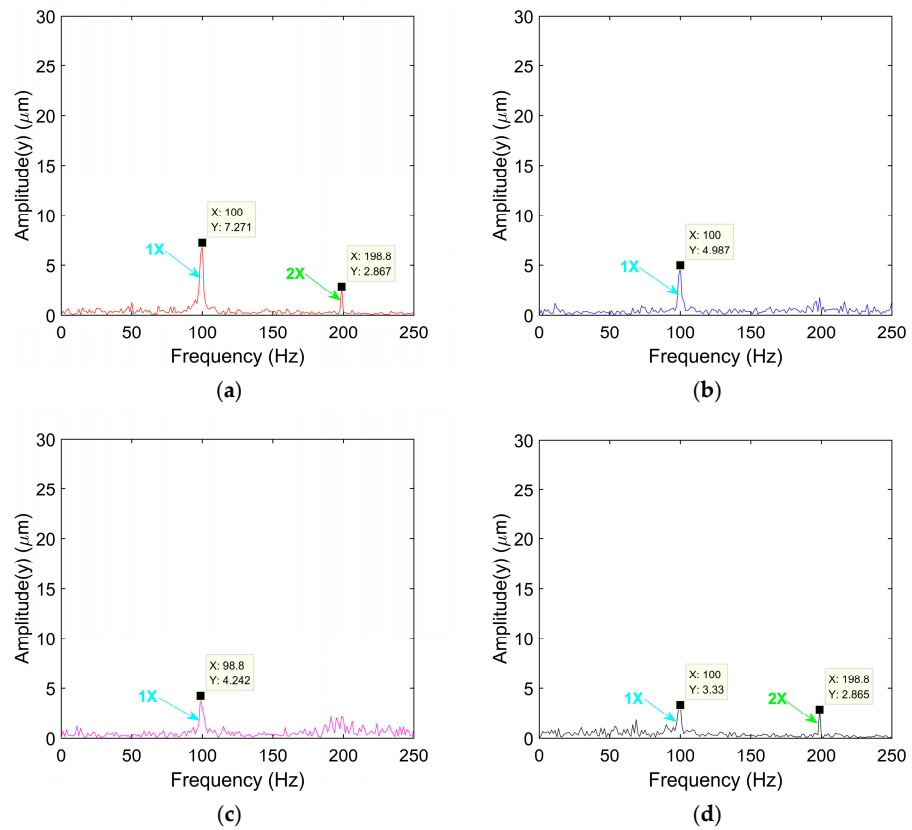**Figure 13.** Displacement spectrum at 5000 rpm under different control displacements. (**a**) Not controlled; (**b**) 0.5 V; (**c**) 1 V; (**d**) 2 V.

Figure 14. Displacement spectrum at 6000 rpm under different control displacements. (**a**) Not controlled; (**b**) 0.5 V; (**c**) 1 V; (**d**) 2 V.
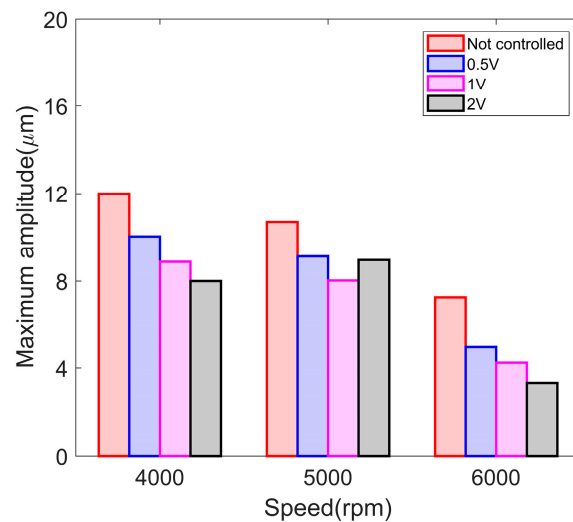

Figure 15. Maximum amplitude of disk response under different control displacements.

Combining the axis trajectory and fundamental frequency amplitude results, angle control and displacement control have better vibration reduction effects at 4000 rpm and 6000 rpm, but at 5000 rpm, the stability of the system is not significantly improved. The general trend is that the stability of the rotor system increases with the increase in the circumferential angle and the radial displacement of the bearing bush. The greater the control amount of the angle and displacement, the smaller the amplitude of the rotor and the smaller the axis track area. By controlling the circumferential angle of the bearing bush, the directional stability of the system can be improved and the vibration can be reduced. It is suitable for application scenarios where it is necessary to control the direction

of the bearing movement, reduce vibration and noise, and improve system stability. By controlling the radial displacement of the bearing bush, the load distribution of the bearing can be directly affected, thereby adjusting the radial force and radial stiffness of the bearing and compensating for issues such as increased clearance caused by friction and wear.

4. Discussions

The control experiment done in this paper is to control two tilting pads at the same time, and the maximum driving voltage used is 2 V. In this work, the number of control pads and the applied driving voltage are also important influencing factors to be considered. Moreover, controlling more pad blocks may require more energy to drive the piezoelectric actuator, a trade-off between balancing vibration suppression and energy consumption. Increasing the driving voltage can increase the displacement of the piezoelectric actuator, thereby causing a larger adjustment range of the bearing pad, but this needs to take into account the clearance of the bearing itself. Piezoelectric actuators demonstrate notable advantages in controlling bearing pad angles, including rapid response, high precision, and wear-free operation. However, they do have limitations such as a restricted displacement range, susceptibility to temperature effects, and a potentially higher energy consumption. On the other hand, in regard to controlling displacement, piezoelectric actuators offer advantages like a larger displacement range, high load capacity, and adaptability to various environments. However, they exhibit slower response speeds and lower displacement precision. Therefore, in practical applications, a careful balance of these pros and cons is essential.

5. Conclusions

On the basis of verifying that two new types of flexible tilting pad bearings have good effects on shock absorption, this paper discusses the influence of piezoelectric control on the vibration performance of two new types of flexible tilting pad bearing systems, and draws the following conclusions through experimental research:

(1) The flexible bearing–rotor test bench was established, and two kinds of structural bearings were designed and manufactured. The circumferential angle of the disk of the angle bearing and the radial displacement of the disk of the displacement bearing are successfully controlled by the piezoelectric actuator, and the axial trajectory and spectrum of the bearing at different rotational speeds are obtained.

(2) The research results of angle control show that the axis trajectory of the piezo-controlled angular bearing–rotor system decreases significantly at 4000 rpm, and the peak displacement of fundamental frequency decreases by 62% at 6000 rpm. This indicates that by controlling the swing angle of the bearing bush, a steeper wedge gap is formed between the bearing bush and the rotor shaft, thereby increasing the oil film pressure and bearing capacity, and suppressing the spindle vibration.

(3) The displacement control results show that with the increase of the radial displacement control amount of the bearing bush, the axial trajectory of the rotor journal becomes smaller and closer to the bearing center. At 6000 rpm, the axis track area decreases obviously, and the peak displacement of the fundamental frequency decreases by 54%. The radial displacement of the bushing reduces the radius clearance of the bearing, changes the damping coefficient and stiffness coefficient of the bearing, and thus adjusts the vibration amplitude of the rotor.

(4) According to conclusions 2 and 3, the vibration performance of two new tilting pad bearing–rotor systems is improved by the piezoelectric control of the bearing's circumaxial angle and radial displacement, and the internal geometric parameters of the bearing are changed, thus laying a technical foundation for the realization of intelligent bearings.

References

1. Delgado, A.; Vannini, G.; Ertas, B.; Drexel, M.; Naldi, L. Identification and Prediction of Force Coefficients in a Five-Pad and Four-Pad Tilting Pad Bearing for Load-on-Pad and Load-Between-Pad Configurations. *ASME J. Eng. Gas Turbines Power* **2011**, *133*, 092503. [CrossRef]
2. Suh, J.; Palazzolo, A. Three-dimensional dynamic model of TEHD tilting-pad journal bearing—Part I: Theoretical modeling. *J. Tribol.* **2015**, *137*, 041703. [CrossRef]
3. Zhang, Z. *Fluid Dynamic Lubrication Theory of Sliding Bearings*; Higher Education Press: Beijing, China, 1986. (In Chinese)
4. Hei, D.; Lü, Y.; Zhang, Y. Nonlinear Dynamic Characteristics of Rotor Supported by Fixed-Tilting-Pad Bearings. *J. Mech. Strength* **2016**, *38*, 940–946. (In Chinese)
5. Amamou, A.; Chouchane, M. Nonlinear stability analysis of long hydrodynamic journal bearings using numerical continuation. *Mech. Mach. Theory* **2014**, *72*, 17–24. [CrossRef]
6. Feng, K.; Liu, W.; Zhang, Z.; Zhang, T. Theoretical model of flexure pivot tilting pad gas bearings with metal mesh dampers in parallel. *Tribol. Int.* **2016**, *94*, 26–38. [CrossRef]
7. Chen, S.; Xiong, W.; Lu, C.; Ma, J. Research on Static and Dynamic Characteristics of Flexure-pivot Tilting Pad Journal Bearings. *J. Vib. Shock* **2018**, *37*, 236–241. (In Chinese)
8. Santos, I. Controllable Sliding Bearings and Controllable Lubrication Principles—An Overview. *Lubricants* **2018**, *6*, 16. [CrossRef]
9. Breńkacz, Ł.; Witanowski, Ł.; Drosińska-Komor, M.; Szewczuk-Krypa, N. Research and applications of active bearings: A state-of-the-art review. *Mech. Syst. Signal Process.* **2021**, *151*, 107423. [CrossRef]
10. Das, A.S.; Dutt, J.K.; Ray, K. Active vibration control of unbalanced flexible rotor-shaft systems parametrically excited due to base motion. *Appl. Math. Model.* **2010**, *34*, 2353–2369. [CrossRef]
11. Silva HA, P.; Nicoletti, R. Rotor vibration control using tilting-pad journal bearing with active pads—Numerical and experimental results. *J. Sound Vib.* **2023**, *546*, 117441. [CrossRef]
12. Santos, I.F. Design and evaluation of two types of active tilting pad journal bearings. In *Active Control of Vibration*; Burrows, C.R., Keogh, P.S., Eds.; Mechanical Engineering Publications Ltd.: London, UK, 1994; pp. 79–87.
13. Bently, D.E.; Grant, J.W.; Hanifan, P.C. Active Controlled Hydrostatic Bearings for a New Generation of Machines. *ASME* **2000**, *2000*, V002T03A011.
14. Bently, D.E.; Eldridge, T.; Jensen, J.; Mol, P. Externally Pressurized Bearings Allow Rotor Dynamic Optimization. *VDI Ber.* **2001**, *1640*, 49–62.
15. Morosi, S.; Santos, I.F. Active Lubrication Applied to Radial Gas Journal Bearings. Part 1: Modelling. *Tribol. Int.* **2011**, *44*, 1949–1958. [CrossRef]
16. Morosi, S.; Santos, I.F. Experimental Investigations of Active Air Bearings. *ASME* **2012**, *44731*, 901–910.
17. Pierart, F.; Santos, I.F. Steady State Characteristics of an Adjustable Hybrid Gas Bearing—CFD, Modified Reynolds Equation and Experimental Validation. *J. Eng. Tribol. Proc. IMechE Part J.* **2015**, *229*, 807–822. [CrossRef]
18. Santos, I.F. On the Adjusting of the Dynamic Coefficients of Tilting-Pad Journal Bearings. *Tribol. Trans.* **1995**, *38*, 700–706. [CrossRef]
19. Santos, I.F.; Nicoletti, R. Influence of orifice distribution on the thermal and static properties of hybridly lubricated bearings. *Int. J. Mech. Sci.* **2001**, *38*, 2069–2081. [CrossRef]
20. Santos, I.F.; Scalabrin, A. Control System Design for Active Lubrication with Theoretical and Experimental Examples. *J. Eng. Gas Turbines Power* **2003**, *125*, 75–80. [CrossRef]
21. Liu, H.; Gong, X.; Wang, J. Vibration Active Control of Rotor System Based on Active Lubricated Tilting-Pad Bearings. *Strength Environ.* **2011**, *38*, 8–17. (In Chinese)
22. Gong, X.C.; Qin, Y.L. Vibration Control of Unsymmetrical Rotating Machinery with an Active Tilting Pad Journal Bearing. In Proceedings of the 2021 IEEE International Conference on Sensing, Diagnostics, Prognostics, and Control (SDPC), Weihai, China, 13–15 August 2021; pp. 260–269.

23. Chasalevris, A.; Dohnal, F. A journal bearing with variable geometry for the suppression of vibrations in rotating shafts: Simulation, design, construction and experiment. *Mech. Syst. Signal Process.* **2015**, *52–53*, 506–528. [CrossRef]
24. Deckler, D.C.; Veillette, R.J.; Braun, M.J.; Choy, F.K. Simulation and Control of an Active Tilting-pad Journal Bearing. *Tribol. Trans.* **2004**, *47*, 440–458. [CrossRef]
25. Da Silveira, A.R.G.; Daniel, G.B. Piezoelectric harvester for smart tilting pad journal bearings. *Energy Convers. Manag.* **2020**, *205*, 112338. [CrossRef]
26. Da Silveira, A.R.G.; Daniel, G.B. Optimization analysis of an energy harvester for smart tilting pad journal bearings considering higher vibration modes. *Mech. Syst. Signal Process.* **2022**, *166*, 108404. [CrossRef]
27. Yan, L.; Yanhua, S.; Lie, Y. Active control of unbalance response of rotor systems supported by tilting-pad gas bearings. *Eng. Tribol.* **2012**, *226*, 87–99.
28. Mizumoto, H.; Arii, S.; Yabuta, Y.; Tazoe, Y. Vibration control of a high-speed air-bearing spindle using an active aerodynamic bearing. In *ICCAS 2010*; IEEE: New York, NY, USA, 2010; pp. 2261–2264.
29. Chang, J.; Ma, J.; Lu, C.; Chen, S. Active Control of Unbalance Response of Rotor Systems Supported by Flexible Hinge Tilting-Pad Bearings. *Comb. Mach. Tools Autom. Manuf. Technol.* **2017**, *2017*, 97–100. (In Chinese)
30. Wang, Q. Dynamic Characteristics and Active Control Study of Dynamic and Static Pressure Flexible Hinge Tilting-Pad Bearings. Ph.D. Thesis, Shandong University, Jinan, China, 2017.
31. Chen, R.; Ouyang, W.; Shi, Z.; Wei, Y.; Yuan, X. Characteristic Analysis and Simulated Test of Hybrid Bearing with the Introduction of Piezoelectric Controller. *J. Shock Vib.* **2016**, *2016*, 6874741. (In Chinese) [CrossRef]
32. Qin, X.; Ji, D.; Wang, X.; Qiu, Z.; Zhu, Y. Simulation Study on Dynamic Performance of Active Control Tilting-Pad Bearing-Rotor System. *Ind. Control Comput.* **2022**, *35*, 100–101. (In Chinese)
33. Girish, H.; Pai, R. Dynamic performance and stability characteristics of a multi-pad externally adjustable fluid film bearing. *Aust. J. Mech. Eng.* **2022**, 1–16. [CrossRef]
34. Huang, G.; Wang, X.; Qin, X.; Zhu, L.; Yi, S. Experimental investigation of dynamic behavior of rotor system with a novel double layers flexible support tilting pad bearing. *Adv. Mech. Eng.* **2022**, *14*, 16878132221116482. [CrossRef]
35. Schweizer, B. Oil whirl, oil whip and whirl/whip synchronization occurring in rotor systems with full-floating ring bearings. *Nonlinear Dyn.* **2009**, *57*, 509–532. [CrossRef]
36. De Castro, H.F.; Cavalca, K.L.; Nordmann, R. Whirl and whip instabilities in rotor-bearing system considering a nonlinear force model. *J. Sound Vib.* **2008**, *317*, 273–293. [CrossRef]